Zero-field magnetic resonance of the photo-excited triplet state of pentacene at room temperature

Cite as: J. Chem. Phys. **113**, 11194 (2000); https://doi.org/10.1063/1.1326069
Submitted: 13 April 2000 . Accepted: 26 September 2000 . Published Online: 13 December 2000

Tran-Chin Yang, David J. Sloop, S. I. Weissman, and Tien-Sung Lin

Zero-field magnetic resonance of the photo-excited triplet state of pentacene at room temperature

Tran-Chin Yang, David J. Sloop,[a] S. I. Weissman, and Tien-Sung Lin[a]
Department of Chemistry, Washington University, St. Louis, Missouri 63130

(Received 13 April 2000; accepted 26 September 2000)

The pulsed EPR free induction decay (FID) signals of the photo-excited pentacene triplet state are reported for three mixed crystals at room temperature: pentacene-h_{14} in *p*-terphenyl, pentacene-h_{14} in benzoic acid, and pentacene-d_{14} in *p*-terphenyl. The recorded FID signals have relatively long decay times of about four microseconds, presumably due to the reduced hyperfine interactions in the zero magnetic field. The time domain FID signals transform to spectral components typically narrower than 500 kHz, allowing us to determine the pentacene triplet zero field splitting parameters to better accuracy than previously reported. Further, a new experimental technique using the high speed magnetic field jumping capability enables us to examine the anisotropic hyperfine and quadrupole interactions. © *2000 American Institute of Physics.* [S0021-9606(00)00648-6]

I. INTRODUCTION

The photo-excited triplet state of the pentacene molecule in a mixed crystal system possesses the following unique properties: high spin polarization, long lifetime, and long spin-lattice relaxation time.[1–5] Thus, the photo-excited triplet state of the pentacene molecule has been utilized as a model system in many spectroscopic studies, such as magnetic resonance spectroscopy of a single molecule,[6–9] spin coherence of a photo-excited triplet state,[10,11] dynamic nuclear polarization (DNP),[12–15] pulsed transient nutation,[16] and the adiabatic passage at the level anti-crossing region (LAC).[17]

In the course of the construction of a fast-field switching spectrometer,[18] and the examination of the spin dynamics at the LAC region,[17] we have developed a specialized field and frequency agile pulsed EPR spectrometer for observing zero and low magnetic field photo-excited triplet signals. Here we present the recorded room temperature ZF EPR FID signals from the photo-excited triplet state of pentacene in *p*-terpheny and benzoic acid crystals in the zero magnetic field. We are able to use the narrow spectral lines obtained by Fourier transform (FT) of the relatively long measured FIDs to determine the zero-field splittings (ZFS) to within about 10 kHz. The transformed linshapes are observed to broaden as the magnetic field is stepped above 0.1 mT. Further, the EPR FID signals display an unexpected long relaxation mechanism that we have not previously observed. The FID signals shift frequency when the laser flashes and microwave pulses occur more frequently than once per second. The shifts in frequency have been measured over several hundred kHz with pulse repetition rates as high as 100 Hz. These observed frequency shifts, possibly due to dynamic spin polarization effects, are presently under further investigation, and will be discussed in a later publication. The ZFS determinations reported here use FID data from experiments with pulse repetition rates low enough to cause less than a few kHz shift of the respective FIDs.

In the past, the optical detection of magnetic resonance (ODMR) technique has been applied to measure the paramagnetic properties of the photo-excited triplet state of organic molecules in the zero field. The ODMR technique measures the changes of the phosphorescence or fluorescence (FDMR) intensity induced by microwave irradiation. On the other hand, EPR techniques measure the magnetization of the electron spin system. Both techniques depend on the phosphorescence lifetime and the degree of electron spin polarization. ODMR appears to be more sensitive than the conventional EPR experiments, especially for short-lived organic triplet states. However, EPR FID data can provide information, which cannot be easily obtained from the optical detection, such as the natural line width, spin–spin relaxation, and phase correlation between photo-excited triplet sublevels.

Here we report the FID measurements of the photo-excited triplet state of pentacene in three systems: pentacene-h_{14} in *p*-terphenyl crystals (PHPT), pentacene-d_{14} in *p*-terphenyl (PDPT), and pentacene-h_{14} in benzoic acid (PHBA). To the best of our knowledge, we believe this is the first EPR FID measurement of a photo-excited triplet state in the zero field at room temperature.

II. EXPERIMENT

The schematic diagram of our zero-field homodyne spectrometer is given in Fig. 1. RF is generated from a frequency synthesizer with 13 dB m output. It is then passed through several frequency doublers to reach the operating frequency, 1.3–1.5 GHz, before going to the circulator. The output signal from the circulator is amplified by a low-noise amplifier (LNA). The operating frequency range of LNA is from 0.6–2 GHz with 35 dB gain and 1 dB maximum noise figure. This amplified signal is then mixed at the balanced

[a]Corresponding authors. Electronic mail: lin@wuchem.wustl.edu or sloop@wuchem.wustl.edu; fax: 314-935-4481

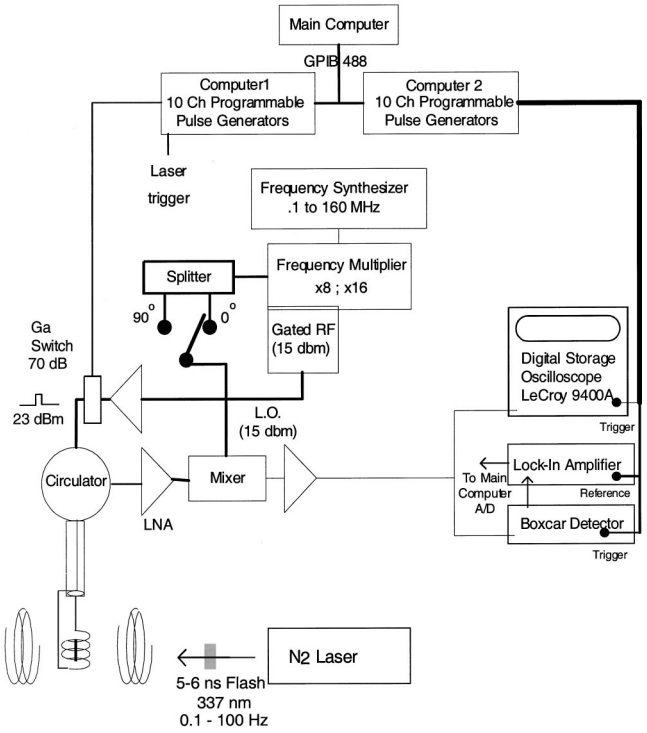

FIG. 1. Schematic diagram of the zero-field spectrometer.

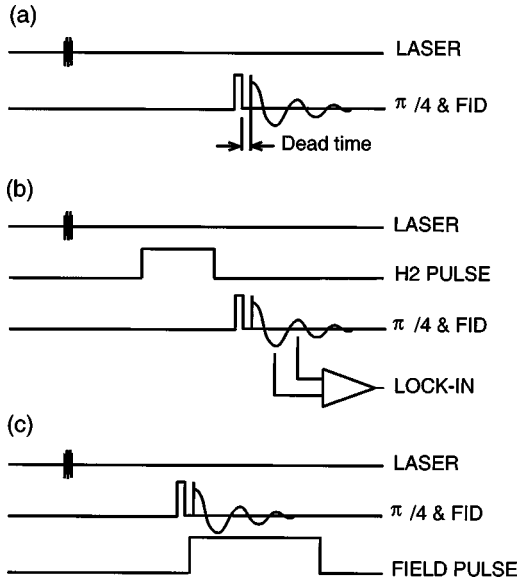

FIG. 2. The pulse sequence for FID acquisition for (a) T_X-T_Z and T_Y-T_Z transitions, (b) the T_X-T_Y transition, and (c) the measurement at a low field by the field-jump pulse.

mixer with the local oscillator frequency, which can be phase switched 90°. The output signal from the mixer is further passed through a 0.0001–1 GHz bandwidth amplifier with 17 dB gain and 6 dB noise figure.

The receiver/transmitter single turn coil is made of #28 copper wire with a diameter of 5.2 mm. Variable capacitors from 0.1–3 pf allow the resonator to be matched to 50 ohm coaxial cable and tuned from 1.3 to 1.5 GHz. This frequency agility enables pulsed EPR measurements of both T_X-T_Z and T_Y-T_Z transitions of the pentacene triplet state, where T_X, T_Y, and T_Z are the zero-field eigenstates with the energy level from the highest to the lowest. The B_1 field strength is about 0.45 G resulting in a 100 ns duration $\pi/4$ pulse. The spectrometer dead time is approximately 0.5 μs following a $\pi/4$ pulse.

For the pulsed EPR experiments reported here, a 100 ns microwave pulse was applied 0.5–3.5 μs after the laser pulse and the FID signal was recorded. The phosphorescence lifetime of the pentacene is about 10 μs at room temperature. The output signal from the spectrometer is fed into a digital oscilloscope (LeCroy 9400). Multiple scan FID averages were sent to the main computer through a GPIB interface. The digitizing resolution of the scope is 10 ns per point and we digitize 10 μs of the FID decays. The time domain data are baseline corrected by subtracting the spectrometer baseline digitized while the laser light is blocked. The baseline corrected FIDs are extended to 160 μs duration by zero filling the FID tail to 16 K points. The FT of these processed FID spectra are then obtained using a MATHEMATICA program. The pulse sequence for the FID acquisition is shown in Fig. 2.

All of the experiments were performed in the zero field at room temperature with a 1 Hz laser repetition rate unless specified otherwise. To ensure the field was truly zero, a CONETIC AA alloy (from the Magnetic Shield Corp.) was used as a magnetic shield with a hole for the laser beam to pass through.

The preparations of single crystals and crystal alignment have been given previously.[2,4] The concentrations of pentacene in *p*-terphenyl or benzoic acid crystals are in the range of $1.0\times10^{-4}-2\times10^{-3}$ mol/mol. We employed a pulsed nitrogen laser ($\lambda=337$ nm, pulse duration$=6$ ns, 1 mJ/pulse, Avco model C950) for excitation. The repetition rate of the laser can be varied from 1 to 100 Hz. All measurements were performed at room temperature.

III. SPIN HAMILTONIAN

The spin Hamiltonian for $S=1$ in the presence of a magnetic field is given by the following equation:

$$H=D(S_Z{}^2-S^2/3)+E(S_X{}^2-S_Y{}^2)+g\beta\mathbf{S}\cdot\mathbf{B}+g_n\beta_n\mathbf{I}\cdot\mathbf{B}+\mathbf{S}\cdot\mathbf{A}\cdot\mathbf{I}. \quad (1)$$

The first two terms, D and E, are the ZFS parameters; arise from the electron spin dipole–dipole interactions. The principal axes of the dipolar tensors x, y, and z of the pentacene are coincide with the long-axis, short-axis, and out-of-plane axis, respectively (see Fig. 3). The third and fourth terms are electron and nuclear Zeeman terms, respectively, where $g(g_n)$ is electron (nuclear) g factor and $\beta(\beta_n)$ is Bohr (nuclear) magneton, and isotropic g factors are assumed. The last term is the electron–nuclear hyperfine interaction, and $\mathbf{A}$ is a hyperfine tensor, which consists of both isotropic and anisotropic interactions.

Let $D=-3Z/2$, $E=(Y-X)/2$; then the dipolar part of the Hamiltonian can be expressed as follows:

$$H_D=D(S_Z{}^2-S^2/3)+E(S_X{}^2-S_Y{}^2)=-XS_X{}^2-YS_Y{}^2-ZS_Z{}^2, \quad (2)$$

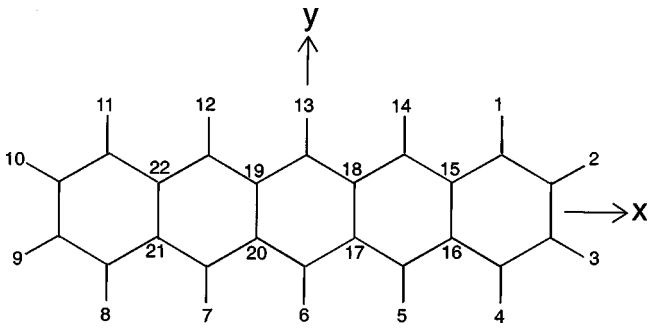

FIG. 3. The axis designation and the numbering of carbon positions of the pentacene molecules.

where X, Y, and Z are the eigenvalues of the triplet state in the zero field. By neglecting the hyperfine and nuclear Zeeman terms, the Hamiltonian of Eq. (1) in the bases of zero-field eigenstates of T_X, T_Y, and T_Z is expressed by the following matrix:

$$H=\begin{bmatrix} X & g\beta B_Z & -ig\beta B_Y \\ g\beta B_Z & Y & g\beta B_X \\ ig\beta B_Y & g\beta B_X & Z \end{bmatrix}, \tag{3}$$

where B_X, B_Y, and B_Z are the **x**, **y**, and **z** components of the external field **B**, respectively.
Note that

$$\begin{aligned} &S_X|T_Y\rangle=|T_Z\rangle,\ \ S_X|T_Z\rangle=|T_Y\rangle, \\ &S_Y|T_X\rangle=i|T_Z\rangle,\ \ S_Y|T_Z\rangle=-i|T_X\rangle, \\ &S_Z|T_X\rangle=|T_Y\rangle,\ \ S_Z|T_Y\rangle=|T_X\rangle, \end{aligned} \tag{4}$$

and

$$S_i|T_j\rangle=0, \quad \text{if } i=j,$$

where $S_i=S_X$, S_Y, or S_Z, and $T_j=T_X$, T_Y, or T_Z.

Thus, $\langle S_i\rangle$ is zero in all directions, which means no angular momentum along three molecular axes in the zero field when the Zeeman and hyperfine terms are neglected.

IV. MAGNETIC MOMENT

The triplet state splits into three sublevels due to the spin dipole–dipole interaction, even in the zero field [see Eq. (2)]. The populations of the triplet sublevels created by the laser light are governed by the molecular symmetry, spin–orbit coupling scheme, and the guest–host interaction. For example, T_X and T_Y substates have equal population after laser excitation for pentacene doped in benzoic acid crystals,[4] but the T_X state is the most populated sublevel for pentacene doped in *p*-terphenyl crystals, the population ratio is 0.76:0.16:0.08 for $P_X:P_Y:P_Z$.[2]

Since the first-order hyperfine interaction is zero in the zero field, the magnetic moments can be evaluated by the following density matrix in the basis set of T_X, T_Y, and T_Z:

$$\mu_j(t)=\mathrm{Tr}[S_j\rho(t)], \tag{5}$$

where

$$\begin{aligned} &\rho(t)=R_{\mathrm{RELAX}}(t)\cdot R_{\mathrm{PULSE}}(\theta_P)\cdot\rho(0)\cdot R_{\mathrm{PULSE}}(\theta_P)^+ \\ &\qquad\cdot R_{\mathrm{RELAX}}(t)^+, \\ &R_{\mathrm{RELAX}}(t)=\exp[-iH_Dt/\hbar], \\ &R_{\mathrm{PULSE}}(\theta_P)=\exp[-iS_j\theta_P/\hbar], \\ &S_j=S_X,\ S_Y,\ \text{or}\ S_Z, \\ &\theta_P=\text{the flipping angle}, \\ &\rho(0)=\begin{bmatrix} P_X & 0 & 0 \\ 0 & P_Y & 0 \\ 0 & 0 & P_Z \end{bmatrix}. \end{aligned} \tag{6}$$

After carrying out the matrix multiplication, Eq. (5) becomes

$$\begin{aligned} &\mu_X(t)=-(P_Y-P_Z)\mathrm{Sin}(2\theta_P)\mathrm{Sin}[(Y-Z)t], \\ &\mu_Y(t)=-(P_Z-P_X)\mathrm{Sin}(2\theta_P)\mathrm{Sin}[(Z-X)t], \\ &\mu_Z(t)=(P_X-P_Y)\mathrm{Sin}(2\theta_P)\mathrm{Sin}[(X-Y)t]. \end{aligned} \tag{7}$$

As shown in the above formulas, the magnetic moments in all three directions are zero before the application of a perturbation pulse at $t=0$. After a microwave pulse, nonzero magnetic moments are created and evolve with time as detected in the FID measurements. The maximum magnetic moment is observed when $\theta_P=\pi/4$.

Furthermore, from Eq. (4), we note that the T_X-T_Y transition is allowed only when we apply the S_Z operator which was first observed by Brandson for phenanthrene in dihpenyl host crystals.[19] We have observed the same phenomena when the S_X operator is applied along the long molecular **x** axis which induces strong T_Y-T_Z transition signal. The signals intensity is expected to be proportional to the population difference between two spin substrates and the pulse rotation angle.

V. ZERO-FIELD FID MEASUREMENTS

Below we shall discuss three different ZF transitions upon the application of $\pi/4$ microwave pulses in three different triplet systems: PHPT, PHBA, and PDPT.

A. ZF T_X-T_Z transition

Previous electron spin echo (ESE) studies showed that the T_X of the pentacene triplet in *p*-terphenyl is the most populated substate.[4,5] Thus, we expected the T_X-T_Z transition to be the strongest signal if we apply the S_Y operator. Experimentally, we must align the coil axis along the **y** axis (the short in-plane molecular axis; see Fig. 3) of the sample. The pulse sequence for the FID acquisition is shown in Fig. 2(a).

We applied the laser pulse at a repetition rate of 1 Hz, and the flip angle of the microwave pulse at $\pi/4$. To avoid recording during the spectrometer dead time, FID signals are recorded starting at 0.5 μs after the $\pi/4$ pulse for 10 μs. Figure 4 shows a typical FID spectrum (a signal average of 200 scans) and corresponding FT spectrum for the PHBA system. Since we do not set the spectrometer frequencies exactly equal to the resonance frequencies, the signal offset frequency could be above or below the homodyne frequency.

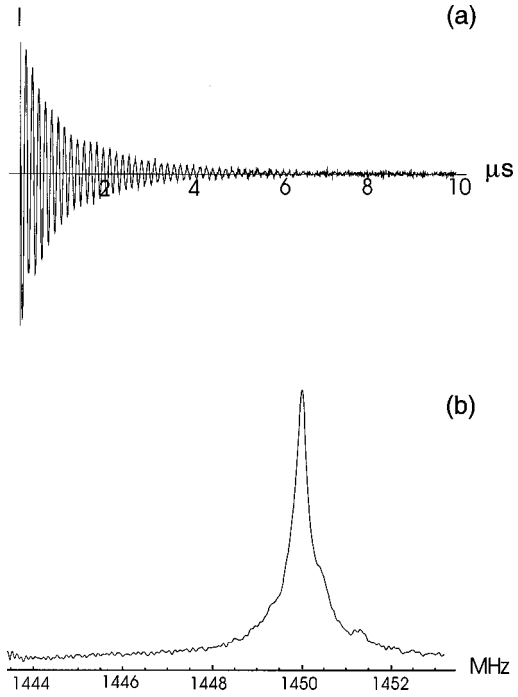

FIG. 4. A typical FID of the photo-excited triplet state of pentacene in the benzoic acid crystal and the corresponding FT spectrum of a zero-field transition ($T_X - T_Z$) at room temperature.

To determine the transformed peak frequency unambiguously, we acquire more than one spectrum with different homodyne frequencies for each transition.

B. ZF $T_Y - T_Z$ transition

When the S_X pulse is applied, we observe the strong $T_Y - T_Z$ transition. Thus, the validity of Eq. (7) is confirmed. Figure 5 displays the FT spectra of both $T_Y - T_Z$ and $T_X - T_Z$ transitions for PDPT and PHPT systems. The peak frequencies for these two transitions are summarized in Table I.

TABLE I. Transition frequencies and D and E values.

Transition		PDPT	PHPT	PHBA
		1447.25		
$T_X - T_Z$ (MHz)[a]		1448.12	1448.93	1450.00
		1448.77[b]		
			1341.43	1339.74
$T_Y - T_Z$ (MHz)[a]		1341.75	1342.23[b]	1340.51[b]
			1343.01	1340.74[b]
				1341.66
$T_X - T_Y$ (MHz)[a]		107.35	107.50	
D	MHz	1395.27	1395.57	1395.30
	cm^{-1}	0.046509	0.046519	0.046510
$\|E\|$	MHz	53.51	53.35	54.69
	cm^{-1}	0.001784	0.001778	0.001823

[a]Within ±0.04 MHz deviation.
[b]Main peak.

C. Low-field (0−2 mT) pulsed field $T_Y - T_Z$ FID

Magnetic field jump experiments investigating the triplet anticrossing spin dynamics have been previously reported.[17,18] We present here what we believe to be a promising experimental technique for using the field jump technology to examine particular hyperfine, quadrupole, and crystal field interactions by pulsing a magnetic field along selected crystal axes during the FID. We observe that the measurable FID shortens dramatically as a magnetic field is applied and it is difficult to observe signals when the magnetic field is greater than 5 mT and no echo is observed when two pulses are applied. We further note that all the measurable spectral components contribute to the ZF FID by tuning the spectrometer over a 20 MHz range and calculating the corresponding FFTs. The pulse sequence shown in Fig. 2(c) allows us to conveniently measure the EPR lineshape in the 0−3 mT magnetic field range. A magnetic field is pulsed along a selected crystal direction with a rise time of less than 10^{-7} s following a $\pi/4$ microwave pulse. The field is stable before the end of the spectrometer dead time, the FID evolves in the programmed field and the digitized signal is

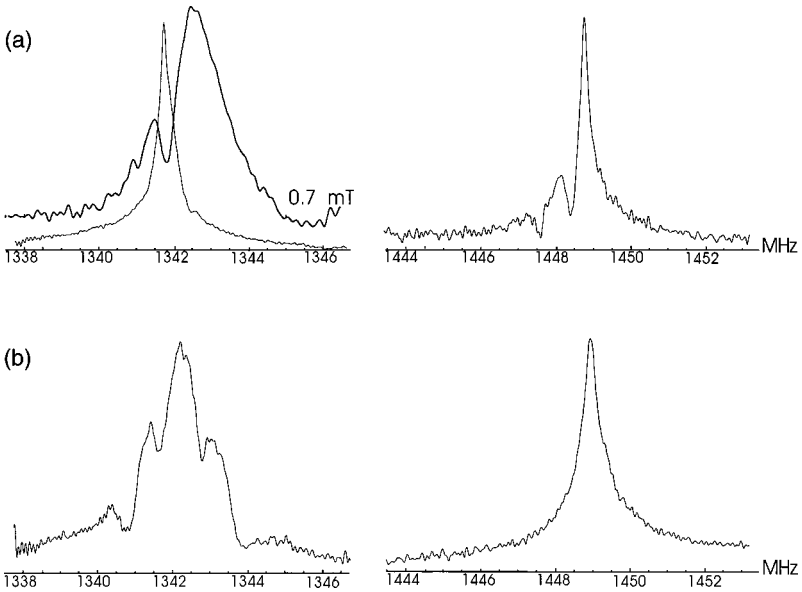

FIG. 5. The FT spectra of zero-field transitions for (a) pentacene-d_{14} in p-terphenyl crystals, left: $T_Y - T_Z$ transition at 0 and 0.7 mT pulsed magnetic field; right: $T_X - T_Z$ transition, and (b) pentacene-h_{14} in p-terphenyl crystals, left: $T_Y - T_Z$ transition; right: $T_X - T_Z$ transition.

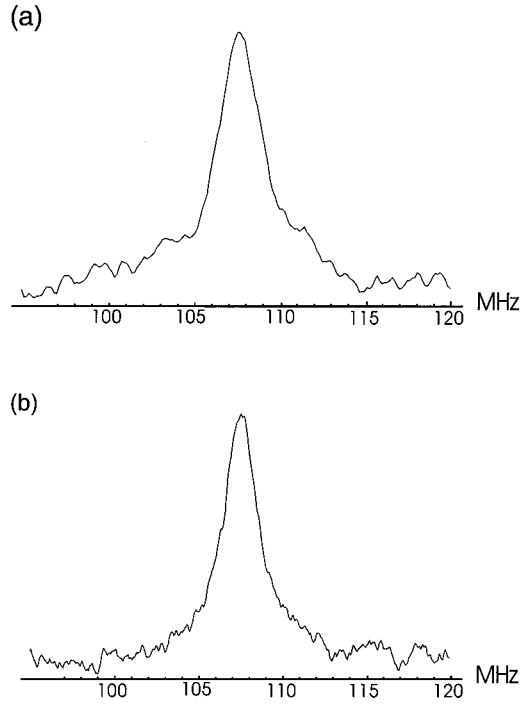

FIG. 6. Plots of FID intensities as a function of RF (H2 pulses) frequencies (T_X-T_Y transitions) for (a) pentacene-h_{14} in *p*-terphenyl crystals and (b) pentacene-d_{14} in *p*-terphenyl crystals.

stored as described previously. Figure 5(a) (left diagram) shows the FT spectrum of the PDPT T_Y-T_Z transition with the field pulsed at zero and 0.7 mT. Line broadening and splitting is clearly visible. We believe such spectral information should provide valuable data in this difficult spectral region (where the applied magnetic fields are on the order of the hyperfine interactions). We are currently applying the density matrix method to simulate these data.

D. ZF T_X-T_Y transition

From T_X-T_Z and T_Y-T_Z transition frequencies, we can calculate the T_X-T_Y transition frequency. The energy gap between T_X and T_Y states in the zero field is slightly greater than 100 MHz. That lies beyond the lower limit of our spectrometer (operating frequency range: 600 MHz–2 GHz). Thus, we employed a different pulse scheme [Fig. 2(b)] to measure the energy separation between these two spin sublevels. There, a 2 μs duration RF pulse (H2) is applied after the laser pulse but before the $\pi/4$ pulse. The RF frequency of the H2 pulse is scanned in the range (95−120 MHz) of the energy gap between T_X and T_Y in a zero field which is similar to an a pulsed ENDOR scheme reported earlier.[20] The intensity is measured by detection at two FID peak positions selected by a boxcar integrator before going into a lock-in amplifier. The repetition rate of the H2 pulse and $\pi/4$ pulse are twice that of the laser pulse and the reference frequency for the lock-in amplifier. The FID intensities as a function of the applied RF frequencies are shown in Fig. 6. The T_X-T_Y transition frequencies are measured to be 107.35 and 107.50 MHz for PDPT and PHPT, respectively.

We further notice that the FID signals for the T_Y-T_Z transition upon the application of 107 MHz of H2 pulse are much stronger than those without an H2 pulse. This result implies that the population rate P_X is larger than P_Y for both PDPT and PHPT, which is consistent with our kinetic data.[5] However, we cannot observe the T_X-T_Y signal for PHBA by this pulse scheme. This may be due to T_X and T_Y having equal population. Yu reported the population ratio of PHBA as $P_X \cong P_Y > P_Z$ from the spin dynamic simulation.[4] The changes of population ratio from $P_X > P_Y$ in PHPT and PDPT to $P_X \cong P_Y$ in PHBA were attributed to possible host effects, such as the phonon structure and the external heavy atom.

VI. CALCULATIONS OF ZFS

The frequencies of T_X-T_Z, T_Y-T_Z and T_X-T_Y transitions are summarized in Table I. We used the main peaks to calculate the ZFS, D and E values. For the T_Y-T_Z transition of the PHBA system, the main peak was taken from the average of the central two peaks. The measured T_X-T_Y transitions are close to the $|2E|$ values calculated from the other transitions. However, the transition frequency measured by this pulse scheme is subject to larger uncertainties because the spectral width is relatively broad.

These values are comparable to those reported previously measured by an x-band pulsed EPR spectrometer.[2] However, our values differ from those reported in the FDMR of a single molecule of pentacene in *p*-terphenyl crystals measured at 1.2 K.[6,7] Their T_X-T_Z and T_Y-T_Z transition frequencies are about 30 and 20 MHz higher than our values, respectively. The discrepancy may be due to the difference in molecular conformation at different experimental temperatures.

The crystal structure study showed that the *p*-terphenyl crystal could undergo a phase transition at 190 K, transforming from a monoclinic form at room temperature to a triclinic one below the phase transition temperature.[21] Furthermore, the *p*-terphenyl molecule changes from a planar conformation at room temperature to nonplanar below the phase temperature. This is also confirmed in the absorption and emission spectra of pentacene in *p*-terphenyl crystals where a multiple sites structure have been observed at low temperatures.[22] Our previous ESE study of PHPT also showed that the system underwent a conformational change when the crystal was cooled below the phase transition temperature.[5] However, a previous ESE experiment at 17 K yielded signal about 14 and 6 MHz higher than those obtained at room temperature for T_Y-T_Z and T_X-T_Z transitions, respectively.[5] Thus, the D and E values measured in ESE experiments are closer to those measured in ODMR or FDMR experiments at liquid helium temperatures. Due to the narrow spectral line width and high signal to noise ratio, the FT spectra can be obtained reproducibly with small uncertainty; estimated to be less than $0.2\times10^{-6}\,\mathrm{cm}^{-1}$ for 10 spectral averages (statistical).

VII. LINE SHAPE ANALYSES

In the zero magnetic field, the first order hyperfine interaction (HFI) between the electron spin of the molecule and proton spins is zero. Thus, one needs only to consider the

second order HFI that could arise from the interaction between different electronic substates. The observed homogenous line width may also arise from a spectral diffusion process of those nuclear spins responsible for the HFI that are allowed to change their spin states while the molecule is in the singlet state, i.e., the nuclear spins can flip freely due to dipole–dipole interactions with surrounding nuclear spins in the singlet manifold.

As shown in Figs. 4 and 5(b), the ZF spectra for the PHBA and PHPT systems have the same spectral features except slight differences in the resonance frequencies. There, one single peak is observed for T_X-T_Z and multiple peaks are resolved for the T_Y-T_Z transition. The multiple peaks may arise from second order hyperfine interactions and the forbidden transitions (see below). Thus, host molecules may not greatly affect the hyperfine interactions, but affect the electronic structure of the guest molecule, as observed through the differences in D and E values.

The observed spectral widths (full-width at half-maximum, $\Delta\omega_{\mathrm{fwhm}}$) for the T_Y-T_Z transitions are 2.2 MHz (0.078 mT) for both PHPT and PHBA, and 0.7 MHz (0.025 mT) for PDPT, a factor of 3 reductions. On the other hand, for T_X-T_Z transitions, $\Delta\omega_{\mathrm{fwhm}}$ are 0.7 MHz for all three samples. The magnetic moment of deuterium is 6.51 times smaller than that of the proton. Thus, the energy shifts or the line widths of PHPT should be 42.4 times greater than that of PDPT by calculating the second order hyperfine interaction in a zero field. The additional broadening may arise from the quadrupole terms contributed by deuterons in the PDPT system (see below).

These values are at least one order of magnitude smaller than those measured at the high magnetic field (such as in the x-band spectrometer) where the anisotropy of the hyperfine interaction often broadens the spectral line. For instance, the typical x-band EPR spectral widths are in the range of 0.6 -1.5 mT for PHPT at liquid helium temperatures[2] and 0.3 -0.4 mT for PDPT.[2,5] However, the line width is also temperature dependent, for instance, $\Delta\omega_{\mathrm{fwhm}}$ is 0.31 mT at room temperature, and 0.45 mT at 164 K for $B_0\|z$ in PHPT.[4,5]

As displayed in Fig. 5(b), the T_Y-T_Z transition for the PHPT system is comprised of an additional structure in contrast to a single peak for the T_X-T_Z transition. However, the spectra for PDPT [Fig. 5(a)] are totally different from those for PHPT and PHBA: one single peak for T_Y-T_Z transition and three resolved peaks for T_X-T_Z transition. The structure may arise from the second order HFI and the forbidden transitions. We also noticed that the spectral line shape is symmetric in our ZF FID measurement. This is in contrast to an *asymmetric* line shape observed in the ZF FDMR of the T_Y-T_Z transition of the pentacene single molecule with $\Delta\omega_{\mathrm{fwhm}}\approx 8$ MHz at 1.2 K.[6–8] We note that $\Delta\omega_{\mathrm{fwhm}}$ reported in the ZF FDMR studies is a factor of 3.5 greater than that we observed in our ZF FID measurements at room temperature.

Even though both FDMR and FID experiments were performed in the zero field, we note there are two major differences between these two techniques.

(1) The FDMR signal arises from the intensity change of the fluorescence, which consists of a density of states including phonons and vibronic states. Thus, FDMR are performed at liquid helium temperatures to achieve an optimal S/N ratio and narrow line width. In contrast, the FID technique measures the magnetic susceptibilities and we perform our experiments at room temperature.

(2) In the FDMR technique, the microwave is applied continuously to the sample throughout the experiment even in the detection period, which can give rise to line broadening. In our zero-field pulsed EPR FID experiments, the spins ''see'' no externally applied fields while the evolving signal is recorded, i.e., no microwave irradiation is present in the detection period of the FID experiments.

Below we examine the energy distributions for both T_X-T_Z and T_Y-T_Z transitions. We shall treat T_X, T_Y, and T_Z states as three eigenstates. Equation (1) can be simplified and split into two parts, unperturbed term H_0 and perturbed term H' (second order hyperfine interaction),

$$H_0=H_D=-XS_X{}^2-YS_Y{}^2-ZS_Z{}^2, \tag{8}$$

$$\begin{aligned}H'=\mathbf{S}\cdot\mathbf{A}\cdot\mathbf{I}=|&(S_XA_{XX}+S_YA_{YX}+S_ZA_{ZX})I_X\\&+(S_XA_{XY}+S_YA_{YY}+S_ZA_{ZY})I_Y\\&+(S_XA_{XZ}+S_YA_{YZ}+S_ZA_{ZZ})I_Z|\,.\end{aligned} \tag{9}$$

The first and second order energy shifts are

$$\delta_n{}^{(1)}=\langle n^{(0)}|H'|n^{(0)}\rangle=0, \tag{10}$$

$$\begin{aligned}\delta_n{}^{(2)}&=\langle n^{(0)}|H'|n^{(1)}\rangle\\&=\sum{}_k|\langle n^{(0)}|H'|k^{(0)}\rangle|^2/(E_n{}^{(0)}-E_k{}^{(0)}),\end{aligned} \tag{11}$$

where $|n^{(0)}\rangle$ is the eigenstate of Hamiltonian H_0, and $E_n^{(0)}$ is its corresponding eigenvalue. $|n^{(1)}\rangle$ is the first order perturbed eigenfunction of state $|n^{(0)}\rangle$. Using these formulas and the previous reported hyperfine tensors elements,[23] the second order energy shifts for the T_X, T_Y, and T_Z can be evaluated, and the energy distribution can be calculated. Similar calculations have been reported earlier.[5–8]

The calculations give a positive energy shift for the T_X-T_Z transition and a negative shift for the T_Y-T_Z transition. This is due to the small denominator $(X-Y)$ in Eq. (11) which dominates the energy shift. These results are similar to the FDMR signals reported for the pentacene triplet at 1.5 K,[6–11] but these calculated values are different from our observed FT spectra.

We further consider the forbidden transitions with simultaneous transitions of electron and nuclear spins, i.e., $\Delta M_S=\pm 1$ and $\Delta M_I=\pm 1$. We shall consider the protonated samples only. The quadrupolar interactions for the deuterated sample will be discussed in the next section. The calculation is carried out similarly to that for the allowed transition. Once we get the energy level distributions, the forbidden transitions are easily computed. The results of the forbidden transitions are similar to those of the allowed transitions. However, we note that the forbidden transitions have broader spectra. This may be due to the fact that one state can excite or de-excite to more than one state. Furthermore, the difference of frequency shifts or the line shapes are not much different from those of the allowed transitions. This is

attributed to the fact that only one of the fourteen protons can change the sign of the calculation, which is not big enough to make the difference between allowed and forbidden transitions. Experimentally, the attenuation of RF power did not yield much changes in the line shape either.

Now, we consider the hyperfine effect from other nuclei, namely ^{13}C's. The natural abundance of ^{13}C is 1.11% and there are 22 carbons on the pentacene molecule. The possibility of finding one ^{13}C in a molecule is about 0.24. From the reported spin densities, the only sites contributing to the energy shifts are from the carbons at positions 5 (7, 12, 14) or 6 (13) (see Fig. 3 for the numbering), which have a higher electron spin density. The hyperfine tensor elements A_{XX}, A_{YY}, and A_{ZZ} for ^{13}C are 34, 34, and 307 MHz, respectively.[24] From these data, the ^{13}C effect on the transition spectra can be calculated. The broadening of spectral width due to ^{13}C for PHPT at positions 5 and 6 are about 1.3 and 15 MHz, respectively.[8] However, the frequency shifts do not change significantly because fourteen protons compensate the ^{13}C effect even though the hyperfine tensor elements of ^{13}C are much larger than those of protons. For the PDPT sample, the frequency shifts are measurable and dominated by ^{13}C because the hyperfine tensor elements of ^{13}C are even much bigger than those of the summation of 14 deuterons.[9] All fourteen deuterons can modulate the frequency shifts. Since we measure the ensemble average, line broadening is expected to arise from the presence of the ^{13}C effect in the deuterated sample.

VIII. QUADRUPOLE INTERACTION AND DEUTERATION EFFECTS ON ENERGY DISTRIBUTION

In this section, we shall examine the deuteration effects in the PDPT system. Previously, we discussed only the effect of the second order hyperfine term. Here, we shall be concerned with the quadrupole interaction. The quadrupole Hamiltonian is given by the following equation:

$$H_Q = \mathbf{I}\cdot\mathbf{Q}\cdot\mathbf{I}, \tag{12}$$

where $\mathbf{Q}$ is the quadrupole interaction operator. Similar to Eq. (2) of Hamiltonian H_D, the Hamiltonian H_Q can be described by the following equation for $I=1$ of the deuterium system:

$$H_Q = -X_Q I_X{}^2 - Y_Q I_Y{}^2 - Z_Q I_Z{}^2, \tag{13}$$

where

$$X_Q = 1/2A(1+\eta), \quad Y_Q = 1/2A(1-\eta), \quad Z_Q = -A,$$

and

$$A = e^2qQ/2,$$

and η is the asymmetry parameter, Q is scalar quadrupole moment, and eq is the field gradient of the $\mathbf{z}$ component. If the principal axis systems of electron dipole–dipole, and quadrupole interactions are coincident, then the energy level diagram for the Hamiltonian H_D+H_Q in the zero field can be found. If the eigenvalues X_Q, Y_Q, and Z_Q are much greater than the hyperfine interaction terms, there could be only one transition frequency for the T_X-T_Z and T_Y-T_Z transitions.

It has been shown that the quadrupole moment depends on the valance electrons, which are related to the molecular wavefunctions, and the electric field gradient is almost determined by the charge distribution on the atom, which is bonded.[25] The quadrupole moment for deuterium is small due to the nature of its valence electron. The e^2qQ of deuterium on the sp^2 hybridization of the carbon atom had been determined by Olimpia *et al.*[26] The calculated value is 0.189 MHz. Previously, we showed the second order hyperfine interaction due to 14 protons is on the order of 2 MHz. Thus, we estimate the second order-hyperfine interaction for deuterium to be ~0.046 MHz (=2/42.4 MHz). The energy splitting arising from the quadrupole interaction should be larger than that from the second order hyperfine interaction by a factor of 4. We therefore attribute the observed line width of the deuterated sample to the quadrupole interaction.

IX. CONCLUSIONS

Zero-field splitting parameters D and E of the photoexcited triplet state of pentacene have been precisely calculated from the FT spectra of the zero-field FID within ± 0.000003 cm^{-1} deviation: $D=0.046509$ and $E=-0.001784\,\mathrm{cm}^{-1}$ for PDPT; $D=0.046519$ and $E=-0.001778\,\mathrm{cm}^{-1}$ for PHPT; and $D=0.046510$ and $E=-0.001823\,\mathrm{cm}^{-1}$ for PHBA. The FT spectra of PHPT and PHBA show similar line shapes. We observe resolved lines in the T_Y-T_Z transition but not in the T_X-T_Z transition. The FT spectra of PDPT are different; three peaks are resolved in the T_X-T_Z transition but a single peak in the T_Y-T_Z transition. The protonated samples have broader measured line widths than the deuterated samples.

The forbidden transitions due to simultaneous electron and nuclear spin flips are not easily separated from the allowed transitions either by the attenuation of the microwave power or from the theoretical calculation. The quadrupole interactions in the PDPT systems are estimated to be larger than the hyperfine interactions by a factor of 4. Thus, the allowed transition frequencies are expected to be mainly determined by the quadrupole terms and the forbidden frequencies should mainly depend on the hyperfine terms. This perturbation method of calculating energy levels yields a similar spectral pattern as that observed in optical detection experiments at liquid helium temperatures, but these spectra clearly differ from the transformed zero-field EPR FID spectra measured at room temperature. We admit that we do not know the origin of this discrepancy, but we plan to employ a density matrix treatment to further simulate the spectra.

ACKNOWLEDGMENTS

We gratefully acknowledge the critical comments provided by the reviewer. This work was partially supported by a grant from the Research Corporation.

[1] A. J. van Strien and J. Schmidt, Chem. Phys. Lett. **70**, 13 (1980).
[2] D. J. Sloop, H.-L. Yu, T.-S. Lin, and S. I. Weissman, J. Chem. Phys. **75**, 3746 (1981).
[3] H.-L. Yu, T.-S. Lin, S. I. Weissman, and D. J. Sloop, J. Chem. Phys. **80**, 102 (1984).

[4] H.-L. Yu, Ph.D. thesis, Washington University, 1982.
[5] J.-L. Ong, D. J. Sloop, and T.-S. Lin, J. Phys. Chem. **96**, 4672 (1992); **97**, 7833 (1993).
[6] J. Köhler, J. A. J. M. Disselhorst, M. C. J. M. Donckers, E. J. J. Groenen, J. Schmidt, and W. E. Moerner, Nature (London) **363**, 242 (1993).
[7] J. Wrahtrup, C. von Borczyskowski, J. Bernard, M. Orrit, and R. Borwn, Nature (London) **363**, 244 (1993).
[8] J. Köhler, A. C. J. Brouwer, E. J. J. Groenen, and J. Schmidt, Chem. Phys. Lett. **228**, 47 (1994); **250**, 137 (1996); J. Chem. Phys. **105**, 2212 (1996).
[9] J. Köhler, A. C. J. Brouwer, E. J. J. Groenen, and J. Schmidt, Science **268**, 457 (1995).
[10] J. Wrahtrup, C. von Borczyskowski, J. Bernard, M. Orrit, and R. Borwn, Phys. Rev. Lett. **71**, 3565 (1993).
[11] R. Brown, J. Wrahtrup, M. Orrit, J. Bernard, and C. von Borczyskowski, J. Chem. Phys. **100**, 7182 (1994).
[12] A. Henstra, T.-S. Lin, J. Schmidt, and W. Th. Wenckebach, Chem. Phys. Lett. **165**, 6 (1990).
[13] D. J. van den Heuvel, A. Henstra, T.-S. Lin, J. Schmidt, and W. Th. Wenckebach, Chem. Phys. Lett. **188**, 194 (1992).
[14] J. Schmidt, T.-S. Lin, D. J. van den Heuvel, A. Henstra, and W. Th. Wenckebach, IUPAC J. Pure Appl. Chem. **64**, 859 (1992).
[15] J. Schmidt, D. J. van den Heuvel, T.-S. Lin, A. Henstra, and W. Th. Wenckebach, Isr. J. Chem. **32**, 165 (1992).
[16] V. Kouskov, D. J. Sloop, S. B. Liu, and T.-S. Lin, J. Magn. Reson., Ser. A **117**, 9 (1995).
[17] V. Kouskov, D. J. Sloop, S. I. Weissman, and T.-S. Lin, Chem. Phys. Lett. **232**, 165 (1995).
[18] D. J. Sloop, T.-S. Lin, and J. J. H. Ackerman, J. Magn. Reson. **139**, 60 (1999).
[19] R. W. Brandon, R. E. Gerkin, and C. A. Hutchinson, Jr., J. Chem. Phys. **41**, 3717 (1964).
[20] D. J. Sloop and T.-S. Lin, J. Magn. Reson. **86**, 156 (1990).
[21] J. L. Baudour, Y. Delugeard, and H. Caileau, Acta Crystallogr., Sect. B: Struct. Crystallogr. Cryst. Chem. **32**, 150 (1976).
[22] R. W. Olson and M. D. Fayer, J. Phys. Chem. **84**, 2001 (1980).
[23] T.-S. Lin, J.-L. Ong, D. J. Sloop, and H. L. Yu, in Pulsed EPR: A New Field of Applications, edited by C. P. Keijzers, E. J. Reijerse, and J. Schmidt (North-Holland, Amsterdam, 1989), p. 191.
[24] H. M. McConnell and J. Strathdee, Mol. Phys. **2**, 129 (1959).
[25] T. Chiba, J. Chem. Phys. **39**, 947 (1963).
[26] P. L. Olimpia, I. Y. Fui, and B. M. Fung, J. Chem. Phys. **51**, 1610 (1969).